Durability assessment of impregnated Glass Fabric Reinforced Cementitious Matrix (GFRCM) composites in the alkaline and saline environments

A. Nobili[a,*]

[a]*Dipartimento di Ingegneria Enzo Ferrari, via Vignolese 905, 41125 Modena, Italy*

Abstract

In this paper, the effect of the alkaline and of the saline environments on prismatic specimens of impregnated alkali-resistant Glass Fabric Reinforced Cementitious Matrix (GFRCM) coupons is investigated. Two types of mortar are considered as representative of a mid-high performance or fine-texture matrix. Coupons are manufactured, cured for 28 days and then submerged in the alkaline or saline solution at constant temperature in a climatic chamber for 1000 hours (aging). Specimens in the control group are retained in the laboratory environment. Mechanical performance of the aged coupons is assessed through tensile testing. A Digital Image Correlation (DIC) system is used to measure the actual specimen deformation. Ultimate strength and elongation, uncracked and cracked matrix elastic moduli, turning point location and failure mechanisms are determined and compared with the control group's through a variance analysis. Statistical support is found for an important reduction in the ultimate strength and elongation, owing to mortar degradation. This result is confirmed by a similar analysis carried out on the single components (mortars and glass fabric) of the composite. Mortar degradation affects failure through favoring a less desirable fabric slip mechanism, as opposed to fabric rupture.

Keywords: Durability, Fabric reinforced Cementitious Material, Alkaline and Saline environment, Impregnated Glass Fiber

*Corresponding author
Email address: andrea.nobili@unimore.it (A. Nobili)

1. Introduction

Fabric Reinforced Cementitious Matrix (FRCM) represents a promising new technology for structural rehabilitation, repair and reinforcing. It differs from the more established Fiber Reinforced Polymer (FRP) matrix composite system in that the matrix is cementitious and therefore highly brittle, as opposed to the ductile polymeric matrix. Although a brittle matrix has a generally negative bearing on the overall mechanical performance, it lends a number of attractive features, such as greater material compatibility with the existing structures, with special regard to cultural heritage (here, for the best practice, the matrix should be tailored on the application), water vapor permeability and fire resistance capability. Furthermore, cementitious matrix relays on a consolidated support from existing building codes and draws from a vast body of experience in production, design and acceptance [15, 11]. FRCM also distinguishes itself from Fiber Reinforced Concrete (FRC) for fibre reinforcing is spatially arranged in a textile and not randomly dispersed in the matrix [13, 9, 14]. In this respect, FRCM resembles Textile Reinforced Concrete (TRC), the main difference being the adoption of mineral mortar instead of concrete for the matrix. The adoption of FRCM confining on cylindrical concrete specimen under compression at high temperature is considered in [19] where a comparison is drawn with carbon FRP systems. It is shown that, conversely to FRCM systems, a small temperature change plays a major role in the performance degradation of FRP. Durability analysis of FRP systems are largely available in the literature in terms of externally bonded material [5], concrete column confining [18] rods [12] and many more [16]. The same abundance cannot be advocated for FRCM composite systems. In [4, 3], durability of FRCM coupons is investigated through tensile testing under a wide array of environmental exposure conditions and a surprising, yet statistically irrelevant, positive effect is found for different mechanical parameters. Besides, [4] provides a nice general introduction to FRCM composite systems.

In this durability analysis, the effect of the alkaline and of the saline environment on the mechanical performance of four types of resin impregnated Glass Fabric Reinforced Cementitious Matrix (GFRCM) laminates is investigated. The performance degradation of the single constituent materials is also investigated to better identify the vulnerable elements in the composite. Two types of commercially available mortar, coded B and M, and one alkali-resistant glass fabric (ar-GF) are considered. The fabric is impregnated with a tixotropic polymeric resin, which promotes adhesion with the matrix. Exposure environments and the aging procedure follow[1] the recommendations in [2]. Three types of mechanical tests are employed, namely

- traction of thin prismatic composite specimens (named coupons) with wedge type clamps;
- traction of the ar-glass fabric;
- three-point bending test of the mortars.

In the first group of tests, the composite is fitted with carbon fabric tabs glued to the coupon ends through epoxy resin to prevent brittle failure under the pressure exerted by the clamps (cfr. [7]). It is observed that the nature of the restraining device has an important bearing on the measured values of the mechanical properties (cfr. the discussion in [6] for TRC), which can be safely compared only under homogeneous testing conditions. However, given that in this study spotlight is set on a comparative assessment, results should take on a broad validity. The second and third group of tests are aimed at characterizing the ar-glass fabric and the mortars, respectively. All materials are commercially available and have been employed in the reinforcing of actual engineering structures, including cultural heritage sites.

[1] As in the current interpretation of the forthcoming Italian regulation.

Characteristic	Unit	M	B
Mean compression strength after 28 days	[MPa]	5.5	6.5
Mean flexural strength after 28 days	[MPa]	2	3
Support adhesion strength after 28 days	[MPa]	0.5	1
Water content	[-]	20%	23%
Aggregate maximum size	[mm]	0.5	0.7
Longitudinal elastic modulus	[GPa]	7	11
Water vapor permeability μ	[-]	10	12

Table 1: Mortars M and B properties

Characteristic	Unit	Value
Specific weight per unit fabric area	[g/cm^2]	220
Fabric square mesh size	[mm]	12
Glass fibre cross-sectional area per unit length	[mm^2/cm]	0.4
Ultimate strength in the principal directions (impregnated)	[MPa]	800
Young modulus in the principal directions (impregnated)	[GPa]	41

Table 2: Mechanical properties of the impregnated glass fibre fabric

2. Materials and method

All specimens considered in this analysis are manufactured using two types of commercially available mortars, named mortar B and M, whose main properties are presented in Tab.1. They are here taken as representative of a mid-high performance (mortar B) or fine-texture (mortar M) matrix. B mortar is rich in hydrated lime and pozzolan while mortar M is constituted by air-hardening lime, pozzolan and marble sand. They both contain glass micro-fibres and binder may be regarded as only partially hydraulic.

Reinforcing is provided by an alkali-resistant glass fibre fabric (ar-GF) with a square mesh (bi-axial reinforcing). Fabric is impregnated by a polymeric resin and its properties are listed in Tab.2.

2.1. Traction test characterization

Prismatic coupons (Fig.1) of resin impregnated 1-ply GFRCM are obtained in a four-stage procedure:

1. a first 3 mm thick mortar layer is laid onto the bottom part of a two-piece polyethylene formwork;

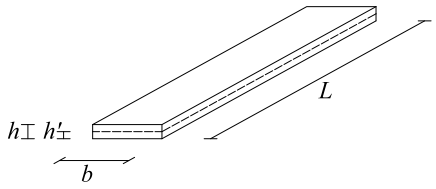

Figure 1: Composite coupon geometry

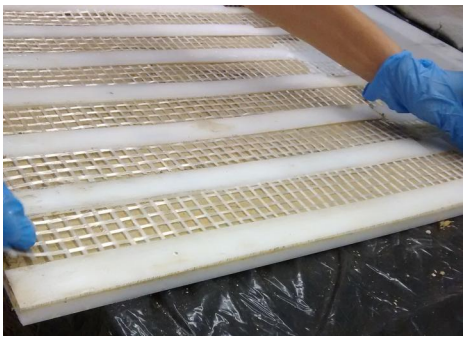

Figure 2: Fabric reinforcement laying out

2. the resin impregnated glass fabric reinforcement is laid on top of the mortar layer (Fig.2), care is taken to prevent air bubbles being trapped under the fabric;
3. the bottom part of the polyethylene formwork is surmounted by the top frame, which provides room for the top mortar layer;
4. a second and final 3 mm thick mortar layer is laid in between the arms of the surmounting formwork;
5. after curing and exposition to the aggressive environment, coupons are fitted at the end surfaces with carbon fiber fabric tabs to prevent fragile rupture due to the wedge grip contact force. Tabs are glued to the coupons with epoxy resin.

Coupon geometry is according to Tab.3.

At all stages, the polyethylene formwork was lubricated to ease safe stripping. Stripping could be safely performed through disassembling the formwork. This procedure avoids cutting from a larger sheet, which may significantly damage the brittle matrix and alter the stress condition. Besides, it affords greater

b	L	h'	h
50	400	3	6

Table 3: Coupon dimensions [mm]

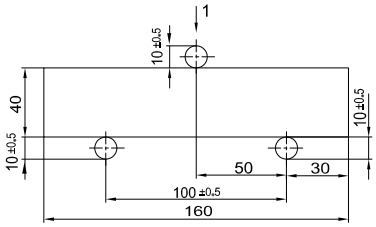

Figure 3: Bending test setup (dimensions are in [mm], cf.[1])

accuracy over the fabric placing (Fig.2). On the overall, 30 composite 1-ply GFRCM coupons have been fabricated for tensile testing, in batches of 5 for the alkaline, saline and control groups.

Coupons have been cured for 28-days in the laboratory environment and then either submerged for 1000 hours ($\approx$ 42 days) in the alkaline or saline solution at a constant temperature of $23 \pm 1°$ C in the climatic chamber for the alkaline or saline group, respectively, or retained in the laboratory environment for the control group ($20 \pm 1°$ C). The alkaline environment is a sodium bicarbonate solution with a PH level of 10. The saline environment is a 3.5% sodium chloride solution, which is the world's ocean seawater average salinity.

2.2. Three-point bending test characterization

Three-point bending tests are carried out according to [1] on homogeneous mortar specimens. Specimens are prismatic with a 40 mm side square cross-section and they are 160 mm long (Fig.3). Specimens are cast in a high precision machined stainless steel form and cured in the laboratory environment for 28 days. Forms were lubricated to ease specimen stripping. Once stripped, specimens are divided in the reference, saline and alkaline groups, each comprising of 5 elements, which are maintained in the relevant environment for 1000 hours, together with the corresponding coupons, in the same solution in the climatic chamber.

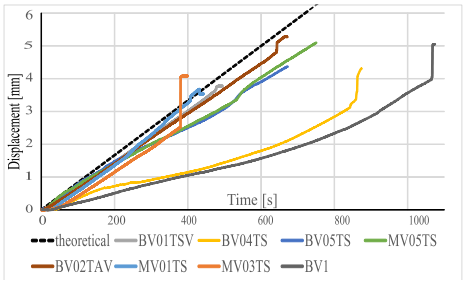

Figure 4: DIC measured coupon elongation curves (solid) vs. theoretical (dashed)

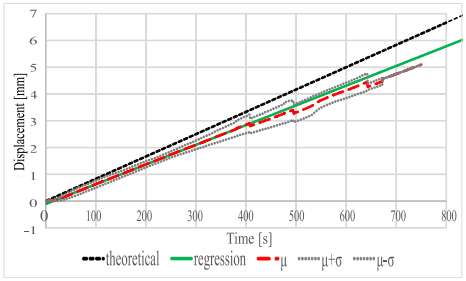

Figure 5: Mean DIC measured coupon elongation (dashed), linear interpolation (solid) vs. theoretical (fine dashed)

3. Traction test results

Traction was performed on an Instron 5567 machine equipped with a 30 kN load cell and pneumatic wedge grips. Traction occurred at a constant elongation rate of 0.5 mm/min. A stereoscopic 3 Mpixel Dantec Dynamics Q-400 Digital Imaging Correlation (DIC) system could efficiently measure the 3D displacement field over one specimen surface during testing at a maximum sampling rate of 15 Hz. Knowledge of the displacement field on the specimen surface in the neighborhood of the wedge grips allowed subtracting from the overall displacement measured by the traction machine the rigid body contribution due to the wedge grip elongation. Fig.4 shows the elongation measured by the DIC system for different specimens and the theoretical curve reproduced by the traction machine. It is clear that a big difference may exist, which has a deep influence on the evaluation of the elastic moduli. The stress vs. traction diagram hereinafter presented are thus deprived of the grip elongation contribution. Fig.5

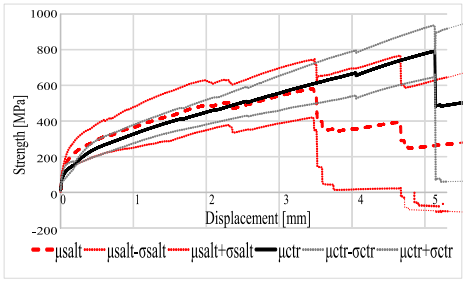

Figure 6: Mean tensile strength curve (dashed) and one standard deviation band (dotted) for the saline group, mortar B, vs. control (solid)

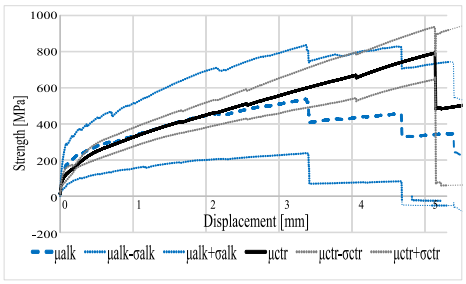

Figure 7: Mean tensile strength curve (dashed) and one standard deviation band (dotted) for the alkaline group, mortar B, vs. control (solid)

shows the mean DIC elongation curve (with the one standard deviation band) and its linear interpolant compared to the theoretical curve: as expected, a growing difference is found between the two.

3.1. Traction strength curves

Fig.6 shows the mean tensile strength curve for the saline and the control groups, for mortar B. As customary, the tensile strength is obtained through dividing the traction load by the specimen *fabric* cross-sectional area A_f (cfr. Tab.2). Displacement is net of the wedge grip rigid body elongation. The mean strength μ is supplemented by the one standard deviation band curves $\mu \pm \sigma$, where σ is the sample estimated standard deviation [10]. As well-known, for a normally distributed population, the percentage of values that lie within a band around the mean μ with a width of one standard deviation σ is 68.27%. Likewise, Fig.7 shows the coupon traction test mean strength curve for the alkaline and the control groups with the relative standard deviations.

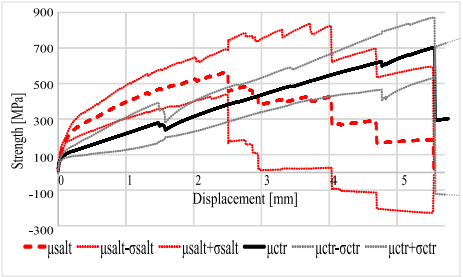

Figure 8: Mean tensile strength curve (dashed) and one standard deviation band (dotted) for the saline group, mortar M, vs. control (solid)

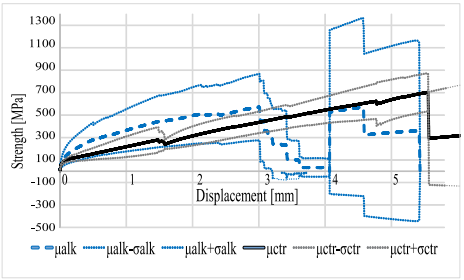

Figure 9: Mean tensile strength curve (dashed) and one standard deviation band (dotted) for the alkaline group, mortar M, vs. control (solid)

Figs.8 and 9 plot the mean strength and the one standard deviation band for the saline and the alkaline groups, respectively, as compared to the control group, for the mortar type M. Tab.4 gathers the mean ultimate tensile strength f_{fu} and elongation ϵ_{fu}, with the corresponding absolute and relative standard deviation. Such values are illustrated in the bar charts of Figs.10 and 11, respectively for the ultimate tensile strength and ultimate elongation. It appears that exposition to the aggressive environment negatively affects the ultimate mechanical performance as well as the amplitude of the population standard deviation. This negative effect on the tensile strength is far more pronounced for the saline environment and the M mortar. The statistical significance of such degradation is discussed in Sec.5. The same outcome is seen for the ultimate elongation although its determination is generally less accurate. The standard deviation band for the ultimate elongation in the alkaline group and mortar M is remarkably narrow.

Mortar	Group	Mean f_{fu}	Std dev		Mean ϵ_{fu}	Std dev	
		[MPa]	abs [MPa]	rel [-]	[-]	abs [-]	rel [-]
M	ctr	782	58	7.4%	1.60%	0.30%	18.75%
	salt	697	175	25.1%	0.95%	0.32%	33.68%
	alk	701	110	15.7%	0.81%	0.04%	4.94%
B	ctr	873	87	10.0%	1.63%	0.29%	17.79%
	salt	746	89	11.9%	1.19%	0.48%	40.34%
	alk	778	112	14.4%	1.43%	0.49%	34.27%

Table 4: Ultimate tensile strength f_{fu} and ultimate tensile elongation ϵ_{fu} with the absolute and relative standard deviation

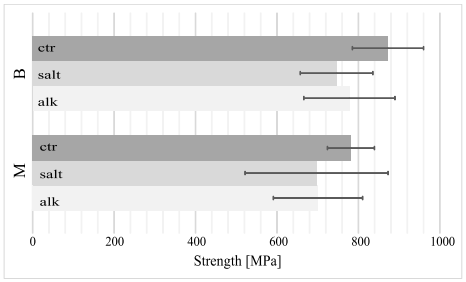

Figure 10: Mean ultimate strength and one standard deviation band

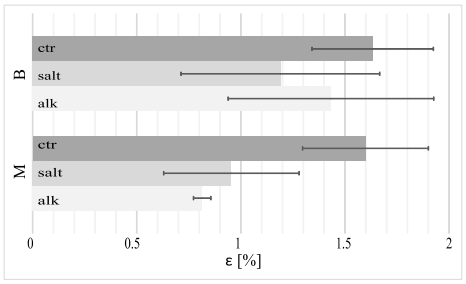

Figure 11: Mean ultimate elongation and one standard deviation band

(a) Fabric failure (b) Fabric slip

3.2. Failure mechanism

Failure occurs according to two principal collapse mechanisms for the glass fabric reinforcement: either rupture or slip in the matrix, respectively Fig.12a and 12b. The failure mechanism is clearly detected by the DIC system, for in the fabric rupture scenario the crack pattern begins with diffuse micro-cracks and it slowly localizes in a final macro-crack (Fig.13). Conversely, the slip mechanism takes place in a single macro-crack which develops at the separation line between the parting fragments. The occurrence of one or the other failure mechanism largely depends on the ratio between the fabric to matrix adhesion strength and the fabric ultimate load. Indeed, fabric failure is almost ubiquitous for the control group, owing to the improved adhesion given by the impregnated fabric, while slippage appears more frequent where the mechanical performance loss due to aging is larger.

3.3. Uncracked and cracked matrix longitudinal elastic moduli

The mean strength curves, corrected to take into account the wedge grip rigid body elongation, may be used to determine the longitudinal elastic modulus for the uncracked, E_1, and the cracked, E_2, matrix. Both moduli are really secant as they are obtained according to the formula [3]

$$E = \frac{f_2 - f_1}{\epsilon_2 - \epsilon_1}. \tag{1}$$

The location of points 2 and 1 differs whether E_1 or E_2 is sought as given in Tab.5.

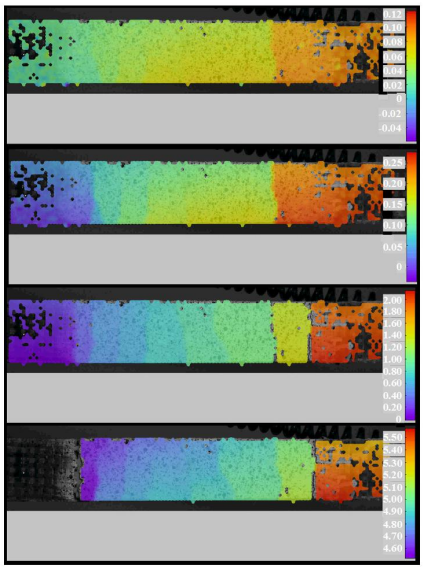

Figure 13: DIC displacement [mm] color map for a fabric failure mechanism

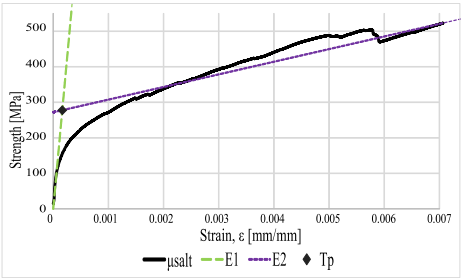

Figure 14: Uncracked and cracked matrix elastic moduli E_1 and E_2

Modulus	Point 2	Point 1
E_1	10%	0
E_2	90%	60%

Table 5: Reference points for the evaluation of moduli E_1 and E_2 as a fraction of the ultimate strength f_{fu}

Mortar	Group	E_1^* [GPa]	E_1 [GPa]	E_2 [GPa]	ϵ_{Tp} [μstrain]	f_{Tp} [MPa]
B	ctr	13	2055	35	132	270
	salt	15	2224	36	124	276
	alk	14	2174	38	111	241
M	ctr	6	960	40	142	137
	salt	12	1886	57	131	247
	alk	12	1902	46	131	249

Table 6: Moduli E_1^*, E_1 and E_2 and turning point (Tp) location

The uncracked and cracked matrix moduli describe the mechanical stiffness before and after the cracking of the brittle matrix: in the former regime the mortar stiffness dominates, owing to its great cross-sectional area A, while in the latter the fabric stiffness takes up the leading role. Accordingly, the modulus E_1^* is introduced

$$E_1^* = E_1 \frac{A_f}{A},$$

where A_f and A are the fabric and the specimen cross-sectional area, respectively. As expected, the elastic modulus E_1^* resembles the matrix elastic modulus, as reported in Tab.1. Different behaviors are possible in the transition between the two regimes, which takes place in the neighborhood of the turning point Tp. The latter is simply defined as the intersection of the lines passing through the points 1 and 2 for the uncracked and cracked regimes. Tab.6 gathers the numerical values for the moduli and the turning point (Tp) location (Fig.14).

4. Single component results

To trace the degradation effect on the single component materials, traction tests have been carried out on the glass fabric (impregnated and dry) and bending tests on the mortar matrix for the alkaline and the saline environment groups as well as the control group.

4.1. Mortar degradation

Bending tests were carried out on mortar prismatic specimens (40 by 40 mm cross-section, 160 mm length) with the same Instron machine in a three-point

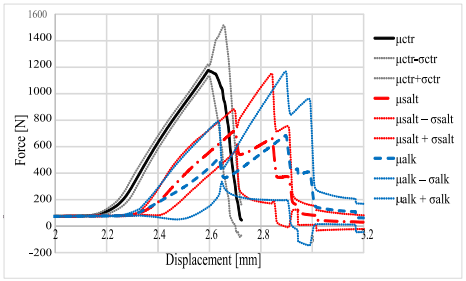

Figure 15: Three-point bending test for mortar B

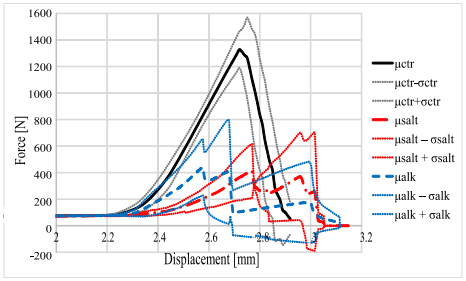

Figure 16: Three-point bending test for mortar M

bending setup (Fig.3) at a displacement rate of 1 mm/min. Specimens were gathered in the control, saline and alkaline groups, 5 specimens apiece. Figs.15 and 16 show the force/displacement curve for mortar B and M, respectively. It is clearly seen that aging has a strong detrimental effect both on the ultimate strength and on the standard deviation amplitude. The bar chart of Fig.17 better focus attention on the ultimate load. The usual brittle failure mechanism at mid-span is found.

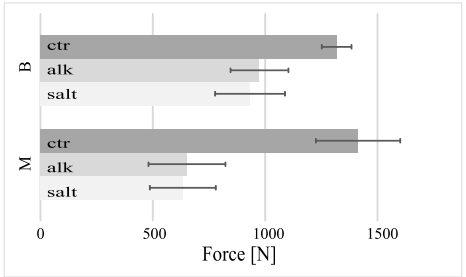

Figure 17: Ultimate load in three-point bonding tests

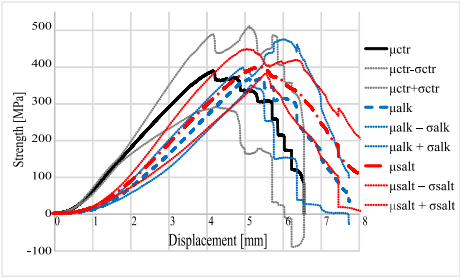

Figure 18: Traction tests for the glass fabric (dry)

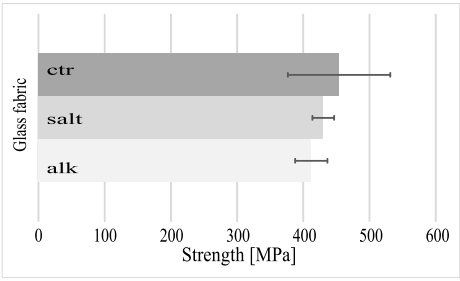

Figure 19: Glass fabric ultimate load

4.2. Glass fabric degradation

Similarly, traction tests were carried out on the glass fiber fabric, again in the control, alkaline and saline groups, 5 specimens per group. Fig.18 shows the mean and the one standard deviation band for each group, at the usual elongation rate of 0.5 mm/min. Ultimate values are gathered in the bar chart of Fig.19. Clearly, there is little statistical difference in the performance of the different groups. Results support the well know fact that ar-glass fabric is a durable reinforcing element in the cementitious matrix. It is perhaps worth mentioning that the standard deviation of the control group is significantly greater than that of the aged specimens, which appear unexpectedly low. While, in this instance, the outcome is most likely due to statistical reasons (too small a population), it is worth pointing out that tensile testing of fabric is usually carried out on impregnated, as opposed to dry, fabric, on the grounds that it gives much more consistent results. Besides, ar-glass fabric still exhibits a complex pattern of performance decay in the alkaline environment of the

Null hypothesis	F	P
Ultimate traction strength for mortar B $\in$ s.p.	1.586	25.2%
Ultimate traction strength for mortar M $\in$ s.p.	0.4540	64.8%
Ultimate traction strength for glass fabric (dry) $\in$ s.p.	0.5927	58.2%
Ultimate bending force for mortar B $\in$ s.p.	17.47	0.1%
Ultimate bending force for mortar M $\in$ s.p.	26.73	0.0%

Table 7: ANOVA test results: F – Fisher-Snedecor ratio, P – Probability confidence, s.p.– same population. The null hypothesis is rejected whenever $F > 1$

cementitious matrix, which is highly sensitive to the pH level [17]. Although such pattern is discernible in our experiments, it has here no statistical appreciation.

5. Analysis of Variance

The statistical significance of the experimental data can be assessed with a one-way ANalysis of Variance (ANOVA) scheme. For a thorough discussion of the ANOVA test (test of significance), see the classic [10, §8.3], while an easy-to-use online resource may be found in [8]. Tab.7 shows the F ratio (Fisher-Snedecor ratio) and the probability confidence P that a given null hypothesis be true. The null hypothesis is that a given set of data, which contains results from the control, saline and alkaline groups, really belongs to the same population, which means that no statistical difference is found between the groups (e.g. the *variance between* is small compared to the *variance within* the groups). In loose terms, P expresses the confidence level that a deviation from the mean is really due to a statistical effect, i.e. it is due to unfortunate sampling within the *same* population. In particular, a low P value is a strong indication of a genuine population difference.

6. Discussion

The results of the ANOVA test give very strong support for a performance degradation of the ultimate bending force for mortars B and M and high support for ultimate tensile strength degradation for coupons with mortar B matrix. Conversely, weak support is given to ultimate tensile strength degradation for coupons with mortar M matrix and for the glass fabric. In general, the small

performance degradation of the fabric reinforcement accounts for the coupon ultimate strength degradation being smaller than the matrix's. As already pointed out, a higher number of specimens in the groups (bigger population size) is required to statistically accept or reject the null hypothesis for the M mortar and the glass fabric.

7. Conclusions

In this paper, the experimental results for tensile characterization of aged impregnated alkali resistant glass Fabric Reinforced Cementitious Matrix (FRCM) composite coupons are presented. Focus is set on the relative performance decay due to the aggressive environments and to which components, within the composite, such decay is mostly due. A Digital Image Correlation (DIC) system is adopted to deprive the theoretical elongation ramp from the wedge grip elongation, thus obtaining the net rate of coupon deformation. Two types of mortar are employed, named B and M, representative of a high-performance and fine-texture matrix, respectively. Coupons are divided into three groups: for the saline and alkaline groups they are submerged in the relevant solution for 1000 hours at controlled temperature in a climatic chamber, the third group being the control (laboratory environment). To track down the effect of the aggressive environments on the single constituent materials, dry glass fabric and prismatic bars of mortar are also exposed to the same solutions as the coupons. Results are presented in terms of tensile strength curves, ultimate tensile strength and ultimate elongation, cracked and uncracked elastic moduli, turning point location, bending force curves, ultimate bending load. As expected, the uncracked matrix modulus resembles the matrix modulus and the cracked matrix modulus the glass fabric longitudinal elastic modulus. A general performance loss is met, which is particularly clear for the mortar bending tests. Conversely, little performance decay is found for the alkali resistant glass fabric. An analysis of variance (ANOVA) is carried out to determine the statistical significance of the results. It provides very strong support for a performance degradation of the ultimate bending force for mortars B and M and high support for ultimate tensile

strength degradation for coupons with mortar B. Most interestingly, such performance decay sharply affects the failure mechanism. Indeed, failure is always ascribed to fabric rupture in the control group, while it drifts towards fabric slippage and delamination in the aged specimens.

Acknowledgments

This study was conducted in collaboration with Ardea Progetti e Sistemi Srl, Bologna, Italy. Financial support form the Fondazione Cassa di Risparmio di Modena, Pratica Sime nr.2013.0662, is gratefully acknowledged. The author is also grateful to Chiara Talami and Stefano Menozzi, who have patiently attended at the correct deployment of the aging process in the climatic chamber.

[1] UNI EN 1015-11, determinazione della resistenza a flessione e a compressione della malta indurita. Technical report, UNI, 2007.

[2] ICC AC434. Acceptance criteria for masonry and concrete strengthening using fiber-reinforced cementitious matrix (FRCM) composite systems. *ICC-Evaluation Service, Whittier, CA*, 2013.

[3] D. Arboleda. *Fabric Reinforced Cementitious Matrix (FRCM) Composites for Infrastructure Strengthening and Rehabilitation: Characterization Methods*. PhD thesis, University of Miami, 2014. Open Access Dissertation. Paper 1282.

[4] D. Arboleda, S. Babaeidarabad, C. DL Hays, and A. Nanni. Durability of fabric reinforced cementitious matrix (FRCM) composites. CICE 2014, 2014. Vancouver, 20-22 August 2014.

[5] J.R. Cromwell, K.A. Harries, and B.M. Shahrooz. Environmental durability of externally bonded FRP materials intended for repair of concrete structures. *Construction and Building Materials*, 25(5):2528–2539, 2011.

[6] J. Hartig, F. Jesse, K. Schicktanz, and U. Häußler-Combe. Influence of experimental setups on the apparent uniaxial tensile load-bearing capacity of

textile reinforced concrete specimens. *Materials and structures*, 45(3):433–446, 2012.

[7] J. Hegger, N. Will, O. Bruckermann, and S. Voss. Load-bearing behaviour and simulation of textile reinforced concrete. *Materials and structures*, 39(8):765–776, 2006.

[8] T.W. Kirkman. Statistics to use. http://www.physics.csbsju.edu/stats/anova.html, 1996.

[9] L. Lanzoni, A. Nobili, and A.M. Tarantino. Performance evaluation of a polypropylene-based draw-wired fibre for concrete structures. *Construction and Building Materials*, 28(1):798–806, 2012.

[10] J. Mandel. *The statistical analysis of experimental data*. Courier Corporation, 2012.

[11] P. K. Mehta and P. JM Monteiro. *Concrete: microstructure, properties, and materials*, volume 3. McGraw-Hill New York, 2006.

[12] F. Micelli and A. Nanni. Durability of FRP rods for concrete structures. *Construction and Building materials*, 18(7):491–503, 2004.

[13] B. Mobasher. *Mechanics of fiber and textile reinforced cement composites*. CRC press, 2011.

[14] A. Nobili, L. Lanzoni, and A.M. Tarantino. Experimental investigation and monitoring of a polypropylene-based fiber reinforced concrete road pavement. *Construction and Building Materials*, 47:888–895, 2013.

[15] A. Nobili and A. M. Tarantino. Unilateral contact problem for aging viscoelastic beams. *Journal of engineering mechanics*, 131(12):1229–1238, 2005.

[16] D. Oehlers and R. Seracino. *Design of FRP and steel plated RC structures: retrofitting beams and slabs for strength, stiffness and ductility*. Elsevier, 2004.

[17] J. Orlowsky, M. Raupach, H. Cuypers, and J. Wastiels. Durability modelling of glass fibre reinforcement in cementitious environment. *Materials and structures*, 38(2):155–162, 2005.

[18] N. Saenz and C. P. Pantelides. Short and medium term durability evaluation of FRP-confined circular concrete. *Journal of composites for construction*, 10(3):244–253, 2006.

[19] T. Trapko. The effect of high temperature on the performance of CFRP and FRCM confined concrete elements. *Composites Part B: Engineering*, 54:138–145, 2013.